



Excitation-independent dual emissions of carbon dots synthesized by plasma irradiation of ionic liquids: Ratiometric fluorometric determination of norfloxacin and mercury(II)

Ching-Bin Ke¹ · Te-Ling Lu² · Jian-Lian Chen²

Received: 23 January 2019 / Accepted: 12 May 2019 / Published online: 25 May 2019
© Springer-Verlag GmbH Austria, part of Springer Nature 2019

Abstract

The capacitively coupled plasma (CCP) discharge of an ionic liquid solution of citric acid produces carbon dots (CDs) with excitation-independent fluorescent dual-emissions peaking at 410 nm and 480 nm. The intensity of the purple photoluminescence at 410 nm increases with (a) the flow rate of O₂ plasma gas supply from 2.0 to 30 standard cubic centimeters per minute (scm), (b) the 2-h exposure of the CDs to 254 nm light, and (c) the 8-h immersion of the CDs in a solution of NaBH₄. The UV exposure and the hydride immersion reduce the fluorescence intensity peaking at 480 nm, which is highest at 5.0 and 10 scm. The two emissive states were revealed by UV–vis absorption, XPS spectra, and time-resolved fluorescence. Control of the O₂ flow rate can simply tune the ratiometric fluorescence of the CCP-CDs. The CDs obtained from 5 and 30 scm O₂ supplies present a high-intensity ratio ($I_{480\text{ nm}}/I_{410\text{ nm}} \approx 3.35$) and a low one (≈ 0.48), respectively. The 480 nm fluorescence of the former CDs is quenched by mercury(II) ions in the 0.2 to 50 μM concentration range. The 410 nm fluorescence of the latter CDs is enhanced by norfloxacin in the 25 nM to 1.0 μM concentration range. The detection limits are 75 nM for Hg(II) and 7.3 nM for norfloxacin.

Keywords Citric acid · Excitation-independent emission · Hydride · Hydroxyl · Intensity ratio · Lifetime · Mechanism · Oxygen · Pyridine · UV exposure

Introduction

Carbon dots (CDs) have been usefully applied in the photochemical, electrochemical, and biochemical fields due to their excellent luminescent properties, their surface functionalization tunability, their biocompatibility, their aqueous dispersibility, and their preparation simplicity and variety [1, 2]. Apart from pursuing an easier synthesis of CDs with a higher emission quantum yield, the ability to tune the fluorescence property of CDs will broaden their application fields. The bottom-up

preparation methods via the carbonization of various organic precursors are more effective to obtain CDs than the top-down methods, for which the cleavage or exfoliation of some macroscopic carbonaceous materials. While most of the bottom-up carbonization is preceded by hydrothermal pyrolysis and microwave-irradiation, we proposed capacitively coupled plasma (CCP) discharges to fabricate the CDs characterized by excitation-independent dual-emission [3].

Dual-emission is helpful to improve the sensitivity of single intensity-based probing in complex samples by providing a reference signal to correct the interferences from instrument fluctuation, environmental changes, and the variance in the probe concentration. Most of the CD-based dual-emissive probes are conjugated with fluorophore counterparts. These counterparts are usually covalently bonded to the probes after the CDs are formed [4–9] or are embedded in the CDs along with the CD's formation [10, 11]. In the nanoprobe, the CD and fluorophore moieties function either as the reference providers or as the probing elements, respectively. They have been used to detect metal ions [4–6, 11], temperature [7], water and moisture [8, 9], hydrogen ions [10], and oxygen [12]. In addition to organic

Electronic supplementary material The online version of this article (<https://doi.org/10.1007/s00604-019-3505-7>) contains supplementary material, which is available to authorized users.

✉ Jian-Lian Chen
cjl@mail.cmu.edu.tw

¹ Department of Beauty and Health Care, Min-Hwei Junior College of Health Care Management, No.1116, Sec 2, Zhongshan E. Rd, Tainan 73658, Taiwan

² School of Pharmacy, China Medical University, No. 91 Hsueh-Shih Road, Taichung 40402, Taiwan

dyes [5, 6, 10, 11], quantum dots [4], Au nanoparticles [7], metal–organic frameworks [8, 9], and even another CDs [12] were used as the joint fluorophores in these studies. Some CDs-based ratiometric fluorescence probes with adjunct fluorophores have been summarized in [13].

By comparison, fewer studies exhibit the intrinsic CD-based ratiometric probing without external fluorophore counterparts involved. There are pH nanoprobe, which choose one pair of excitation/emission wavelengths as a reference basis and another pair as the signal response from a series of excitation-dependent emissions of hydrothermal CDs [14, 15]. Otherwise, a CD exhibiting excitation-independent emissions at two wavelengths is used to detect heparin in medicinal solutions [16]. Although excitation at two different wavelengths is necessary for these studies, the conjugation with fluorophores and the concerns for the uncertainty of the molar ratio of the CD to fluorophore between the synthesis batches are unnecessary.

In the study, the excitation-independent dual-emissions of the CDs was obtained from the CCP discharge of ionic liquid solutions of citric acid. The tunability of the ratio between the fluorescence intensities was realized through changing the CCP parameters and through post-treating the CCP-synthesized CDs with UV-light and NaBH₄ reducing agent. The CCP parameters included the flow rate of the O₂ plasma gas, the radio frequency power, and the power duration. Through UV–Vis absorption, X-ray photoelectron spectroscopy, and static and time-resolved fluorescence, the surface states and emission mechanism of the CDs were investigated in depth. The application of the tunable CDs in the ratiometric determination of metal ions, flavonoids, and antibiotics was also presented.

Experimental

Materials and chemicals

The citric acid (CA), glucose, lactose, ascorbic acid, uric acid, and tetracycline were purchased from Acros Organics (<https://www.acros.com/>). L-tyrosine, L-serine, and 1-ethyl-3-methylimidazolium dicyanamide ([EMIM]N(CN)₂) were obtained from Sigma-Aldrich (<https://www.sigmaaldrich.com/>). Nine flavonoids (5-methoxyflavone (Met), hesperidin (Hpd), naringin (Nag), catechin (Cat), epicatechin (Epi), hesperetin (Hpt), daidzein (Dai), naringenin (Nar), and quercetin (Que)) were purchased from Sigma-Aldrich. All metal and phosphate salts were of analytical grade and were obtained from Sigma Aldrich and Acros Organics.

Synthesis, posttreatment, and the characterization of carbon dots (CDs)

The capacitively coupled plasma (CCP) system (Femto SRS, Diener electronic GmbH + Co. KG, Ebhausen,

Germany) used for carbonation of the mixtures of citric acid (50, 100, 200 mg) and [EMIM]N(CN)₂ ionic liquid (500 μL) was described in detail in the previous paper [3]. The CCP operation parameters, including radio-frequency power (13.56 MHz, 0–100 W), duration time, and flow rate of the plasma inlet gas (0–50 sccm), are manually adjustable in the system. After CCP treatment, the sticky product was rinsed with 1.0 mL of H₂O, centrifuged at 6000 rpm for 30 min, and dialyzed against ultra-pure water through a molecular weight cutoff membrane (500–1000 Da, Float-A-Lyzer G2, 1 mL capacity, Spectrum Laboratories Inc., CA, USA) for 5 days. Finally, the dialyzed solution was adjusted to 2.5 mL by water and diluted with 100 parts of water for fluorescence measurement. Some of the dialyzed solution obtained from the CCP treatment with a 10 sccm O₂ inlet was treated with UV-light (254 nm, 15 W) exposure in a cabinet (C-70G Chromato-Vue, UVP, LLC, CA, USA) and 0.5 M NaBH₄ reduction.

The dialyzed and post-treated CD solutions were characterized by a UV-Vis spectrometer (Lambda 35, Perkin Elmer, MA, USA), spectrofluorometer (LS55, Perkin Elmer, MA, USA), and a time-correlated single photon counting system (TCSPC, TimeHarp 260 PICO, PicoQuant GmbH, Berlin, Germany). The TCSPC system was equipped with a PLS 330 and PLS 370 (PicoQuant GmbH, Germany) providing 335 ± 10 nm and 380 ± 10 nm pulse LED sources, respectively. FluoFit software (PicoQuant GmbH, Germany) was used to fit the fluorescence decay profiles. Parts of the CD solutions were dried through the evaporation of water at 70 °C in a vacuum oven for 1 day for X-ray photoelectron spectroscopy (ULVAC-PHI PHI 5000 VersaProbe, Physical Electronics, MN, USA).

Fluorescence measurement

A 20 μL of the diluted CD solution was added to each sample in a 3.0 mL of phosphate buffer (50 mM, pH 7.0) to measure the fluorescence intensities (*I*) at 410 nm (excitation at 330 nm) and 480 nm (excitation at 390 nm). These *I* values were compared with those (*I*₀) observed in the blanks to evaluate the quenching effect (*I*/*I*₀) × 100% on the samples and to further establish the plots of *I*_{480 nm}/*I*_{410 nm} (or *I*_{410 nm}/*I*_{480 nm}) versus concentrations of the analytes, Hg²⁺, and norfloxacin. The sea water matrices collected from the east coast of Taiwan were filtered through Whatman no.1 and kept at 4 °C before spiking with Hg²⁺. Prior to spiking norfloxacin in milk, the proteins in the milk were removed by acidifying the milk with 0.2 M HCl to pH 4.7 and centrifuging the acidified milk at 5000 rpm for 10 min.

Results and discussion

Effects of oxygen and capacitively coupled plasma (CCP)

Figure 1(a) shows the fluorescence spectrum of the CDs obtained from CCP discharge of the ionic liquid ([EMIM]N(CN)₂) solution of CA in the standard conditions (CA of 100 mg, RF power of 90 W, treatment of 30 min, and O₂ flow of 10 standard cubic centimeters per minute; sccm) used in our previous study [3]. Referring to the standards, some changes in the O₂/CCP parameters would affect the fluorescence and UV–VIS absorption spectra of the formed CDs with excitation-independent dual-emission, as shown in Table S1 in the [electronic supplementary material](#) (ESM). Among the parameters, the O₂ flow rate can more easily control the formation of the CDs than the other parameters, which are discussed in the ESM.

As the O₂ volume flow rate changed from the standard 10 sccm (standard cubic centimeters per minute) to 2.0, 5.0, 20, and 30 sccm, the $\lambda_{\text{ex, max}}$ (390 nm) and $\lambda_{\text{em, max}}$ (480 nm) remained unchanged, but the I_{max} values were clearly reduced except for those of the 5.0 sccm sample, as shown in Table S1. The O₂ supply rates of 5.0 and 10 sccm were optimum for the formation of the 480 nm emissive CDs at the 390 nm excitation, as shown in Fig. 1(b). For the 20 sccm and 30 sccm

samples, another strong emission peak appeared at nearly 410 nm with the 330 nm excitation. As shown in Fig. 1(c), two emission bands, which were centered at 410 nm and 480 nm and were excitation-independent within their respective excitation ranges of 310–350 nm and 370–430 nm, coexist in the CDs obtained at 30 sccm. Figure 1(d) shows the 410 nm emission is increased with the increase of the flow rate of the O₂ supply from 2 sccm to 30 sccm. These dependencies of emission on flow rate can be used to synthesize a CD with dual (purple and blue-green) emissions. Figure 2 shows that the ratio of photoluminescence (PL) intensity at 480 nm to that at 410 nm ranges from 0.48 to 3.35.

The observed changes in the UV–Vis absorption, XPS spectra, and time-resolved fluorescence suggest the presence of different emissive states in the CDs obtained from different O₂ flow rates. As shown in Table S1 and Fig. S1, the UV–Vis absorption peaks at approximately 380 nm for the 20 sccm and 30 sccm CDs disappeared but their absorptions at wavelengths shorter than 300 nm became stronger when compared with the 2, 5, and 10 sccm samples. It is believed that the stronger optical absorption in the 230–320 nm range is ascribed to the π – π^* transition of the conjugated C=C bonds in typical CDs, while the absorption at higher wavelengths is attributed to the n – π^* transition of C=O, C=N or other groups connected with the C=C bonds [17]. Therefore, for the 20

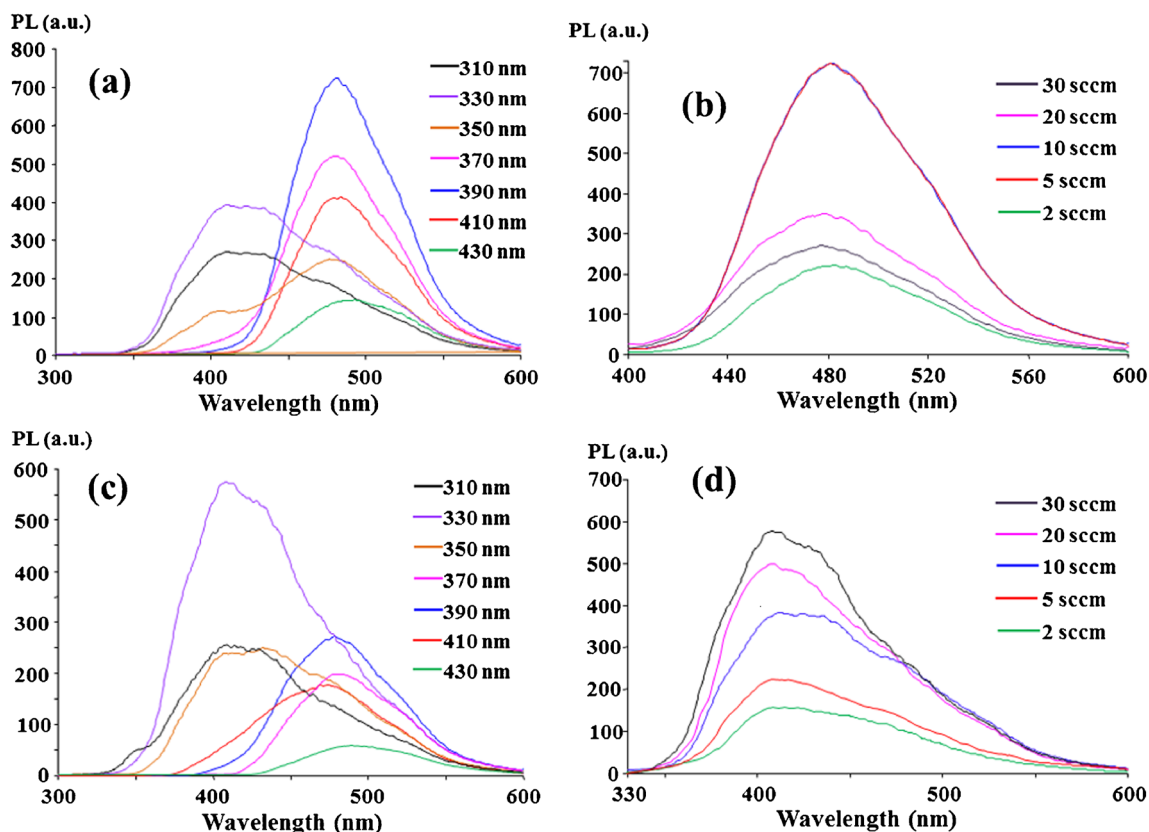
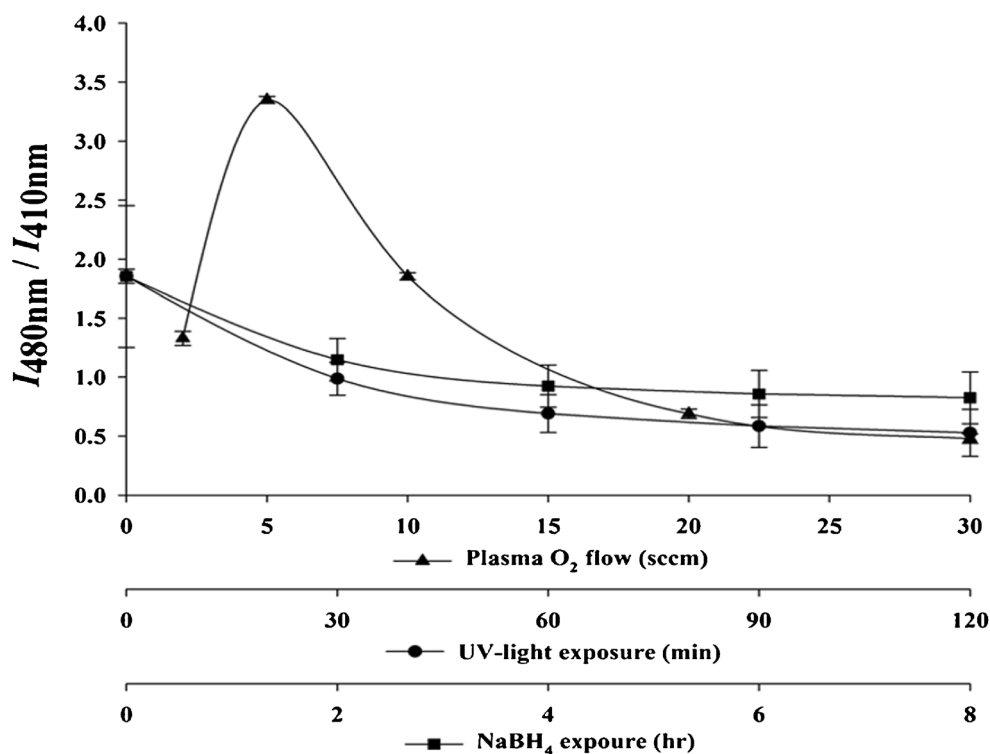


Fig. 1 The fluorescence spectra of the CDs obtained by O₂/CCP at a flow rate of 10 sccm (a) and 30 sccm (c) and the effect of O₂ volume flow rate in CCP processes on the fluorescence spectra at 390 nm (b) and 330 nm (d) excitations

Fig. 2 The dependence of the ratio of fluorescence intensities at 480 nm to that at 410 nm on the O₂ volume flow rate, UV-light exposure time, and NaBH₄ treatment duration



sccm and 30 sccm CDs, the increase in the 410 nm emission, as shown in Fig. 1(d), was related to the π - π^* transition and the decrease in the 480 nm emission, as shown in Fig. 1(b), was related to the n - π^* transition.

To clarify the changes in the surface groups, the deconvolution of the C1s, N1s, and O1s peaks in the XPS spectra of the 10 sccm and 30 sccm samples were tabulated in Fig. S2. Compared to the referred peak of C-C/C=C bonds at 284.6 eV, the change in the peak area of the C-N bond at 285.6 eV from the 10 sccm sample to the 30 sccm sample is obscure, but the increases in the peak areas of the C-O bond at 286.6 eV, C=O/C=N bonds at 287.6 eV, and COOH bond at 288.7 eV are obvious. The increases were related to the greater amount of O₂ supplied to the CCP chamber, and thus produced the more oxygen-connected bonds on the CDs. This relationship was further supported by the enlarged peak areas of the C=O bonds at 530.7 eV and C-OH/C-O-C bonds at 532.3 eV in the O1s deconvolution spectra and by the enlarged peak areas of the oxidized pyridinic nitrogen (NO_x) at 404.0 eV in the N1s deconvolution spectra. In the N1s deconvolution spectra, the peak area of the pyrrolic (C₂N-H) and pyridinic (C-N=C) nitrogens, located at 400.2 eV and 399.5 eV, respectively, is decreased, as the peak of graphitic nitrogen (C₃N) at 401.9 eV is considered to be a referred peak. Conceivably, the increase in the oxygen-connected groups is related to the increased 410 nm emission, while the decrease in the nitrogen-connected groups is related to the decreased 480 nm emission.

The lifetimes of the 410 nm ($\lambda_{\text{exc}} = 335 \pm 10$ nm) and 480 nm ($\lambda_{\text{ex}} = 380 \pm 10$ nm) emissions for 5, 10, and 30 sccm CDs were obtained from TCSPC measurements with monoexponential decay fitting and are collected in Table S2. It indicates that the lifetimes, $\tau_1 = 1.5\text{--}1.6$ ns for the 410 nm emission (or the oxygen-connected emissive states) and $\tau_2 = 5.4\text{--}5.5$ ns for the 480 nm emission (or the nitrogen-connected emissive states), were independent of the O₂ flow rate but were dependent on the CD composition. That is, the composition of the surface groups was not affected by the flow rate, but the flow rate adjusted the ratios between the surface groups. Using a 335 ± 10 nm light source to examine the decay curves at 480 nm PL, the changes in the ratios with O₂ flow rate were observed by analyzing the lifetimes with biexponential tailfits, $I(t) = A_1 e^{(-t/\tau_1)} + A_2 e^{(-t/\tau_2)}$. As shown in Fig. S3, the amplitude of the $e^{(-t/\tau_1)}$ component percentage ($A_1\%$) increases with the flow rate while the percentage of the $e^{(-t/\tau_2)}$ component ($A_2\%$) decreases with the flow rate. Here, the increase in the τ_1 component was correlated significantly with the increased oxygen-connected groups, and the decrease in τ_2 component was correlated with the decreased nitrogen-connected groups. The decay curves were plotted in Fig. S3 and their fitting parameters were tabulated in Table S2, showing that the τ_1 (1.5~1.6 ns) and τ_2 (5.2~5.6 ns) values fitted by biexponential tailfits were close to those fitted by monoexponential decays. Therefore, parts of the oxygen-functional groups contribute to the 480 nm emission, and the electrons excited by 335 nm are quickly transmitted to the nitrogen-functional groups.

In detail, the PL mechanism is described in Fig. 3. The 410 nm emission was excited from the intrinsic π domain of CD core and then emitted from the surface states incorporating the oxygen-based groups with edge carbons of the core [17]. The excitation for the 480 nm emission was mainly attributed to the $n-\pi^*$ transition of the nitrogen-based groups in emissive fluorophore molecules, which might be bound with the carbogenic domains or exist individually, as the 480 nm emission was found in the solutions inside and outside of dialysis membrane [3, 18, 19]. It supported the finding that the introduction of nitrogen to the CDs would form lower energy surface states with redshifted emission [20, 21]. The longer lifetime of the nitrogen-based emissive states than the oxygen-based ones was due to bulky molecular fluorophores rather than surface states or traps.

Posttreatment with UV-light exposure

Most of the studies on the stability of new CDs are processed in mild conditions, such as changes in pH and salt concentration, but few are treated in severe ones, such as UV-light exposure and hydride reduction, both of which may modify the surface groups and, thus, alter the fluorescence spectrum. Hydroxyl radicals produced from the photolysis of water under UV-light irradiation would destroy the molecular states or N-doped sites of the CDs and lead to PL quenching [22, 23]. Moreover, UV-light would initiate the carbonization of the emissive pyridone-based molecules and would cause photobleaching [18]. In the study, the quenching occurred at the 480 nm emission, as shown in Fig. 4(a), whereas the photocarbonization slightly raised the 410 nm emission, as shown in Fig. 4(b). Therefore, the ratio of PL intensity at

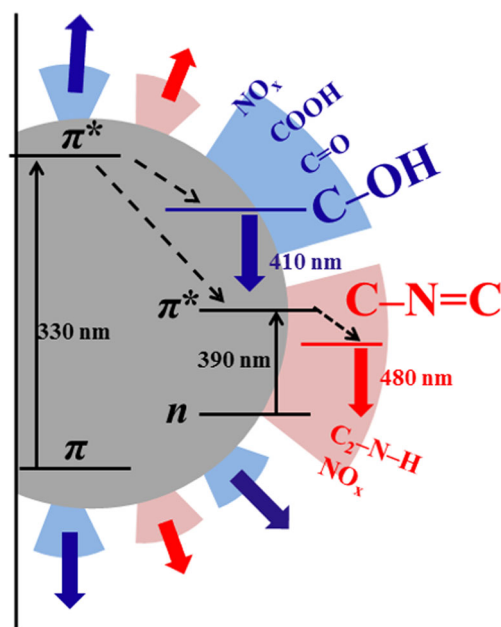


Fig. 3 The fluorescence mechanism

480 nm to that at 410 nm was reduced from 1.854 to 0.527 by a two-hour UV-light exposure, as shown in Fig. 2.

After two-hours of UV-light exposure, the UV-Vis absorption spectra of the CDs demonstrated that the destruction of the N-doped molecular states diminished the $n-\pi^*$ absorption at 380 nm, and the carbonation reinforcement in the sp^2 carbon network slightly strengthened the $\pi-\pi^*$ absorption near 280 nm, as shown in Fig. S1. In addition, the XPS spectra show the diminution of the pyrrolic and pyridinic groups and the strengthening of C-O, C=O, COOH, and NO_x groups in Fig. S2. These changes in spectra were similar to those found in the 30 sccm/ O_2 CDs as the oxidative oxygen species were highly reactive with the intrinsic CDs. The TCSPC data supports the similarity, where either the monoexponential or biexponential decay fittings were fitted, as shown in Fig. S3 and Table S2.

Posttreatment with $NaBH_4$

Some CDs are reduced by $NaBH_4$ to transform the nonradiative epoxy and carbonyl surface groups to hydroxyl ones with PL enhancement and blueshifts as a result of the enrichment of the electron density of the π structure and suppression of the nonradiative recombination of localized electron-hole pairs [24–26]. These CDs are not such as the studied O_2/CCP CDs exhibiting two excitation-independent emissions. In the study, the 480 nm emission is decreased with the duration of the $NaBH_4$ reduction, while the 410 nm emission is increased with the duration, as shown in Fig. 4(c, d). The ratio of the PL intensity at 480 nm to that at 410 nm declined from 1.854 to 0.824 over an eight-hour reduction, as shown in Fig. 2.

For the eight-hour reduced CDs, the decline in the UV-Vis absorption peak near 380 nm reflected the decrease in the n states constituted by the nitrogen-based groups and the decrease in the following 480 nm emission, as shown in Fig. S1. The hydride reduction converted the pyridinic groups to pyrrolic ones in the fluorophore structure, as the pyridinic peak in XPS N1 s spectra is smaller and the pyrrolic peak is larger in Fig. S2. Therefore, the 480 nm emission was chiefly related to pyridinic surface groups. On the other side, the hydride reduction converted the carbonyl surface groups to the hydroxyl ones as the shrinkage of C=O bonds and the growth of C-O bonds are shown in the C1s and O1s spectra in Fig. S2. The 410 nm emission, caused by the $\pi-\pi^*$ transition and oxygen-based groups, would be chiefly related to hydroxyl surface groups. Because there is no effect on the conjugated C=C bonds, the UV-Vis absorption peak near 230–320 nm is not altered by the reduction. Upon checking the TCSPC data in Fig. S3 and Table S2, the reduced CDs possessed a higher A_1 component for the increased hydroxyl groups and a lower A_2 component for the decreased pyridinic ones than the original 10 sccm CDs.

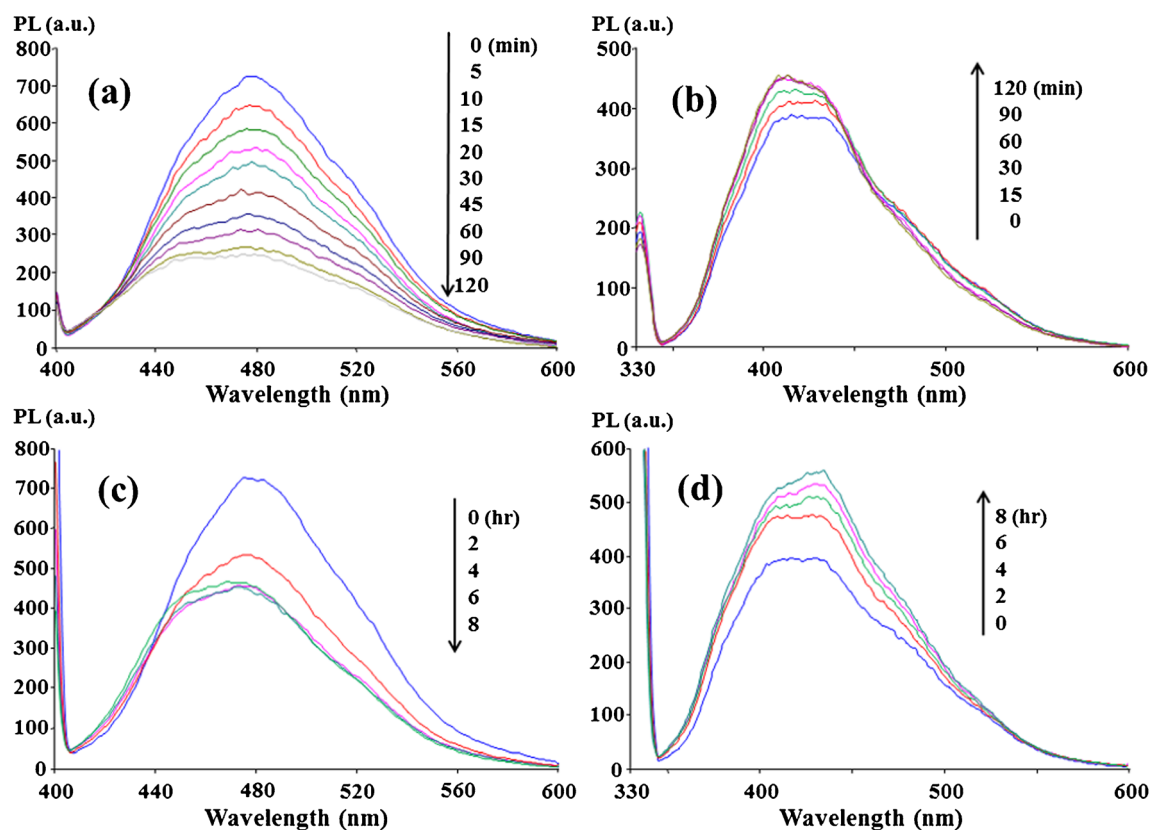


Fig. 4 Dependence of the fluorescence spectra of the CDs treated with UV-light (a, b) and NaBH_4 (c, d) on the treatment duration. Excitation wavelength: 390 nm (a, c) and 330 nm (b, d)

Fluorescent probing

The surface composition of the CDs determines their fluorescence spectra and subsequent probing applications. As shown in Fig. 2, the control of the O_2 flow rate during the formation of CDs by CCP processes was more capable of causing smaller changes in the $I_{480\text{ nm}}/I_{410\text{ nm}}$ ratio or the surface composition or of creating a wider ratio range than of tuning the UV-light or NaBH_4 exposure time following the CD formation. Here, the CDs (CD-5 and CD-30) forming at 5 and 30 sccm O_2 flow rate and possessing the extreme $I_{480\text{ nm}}/I_{410\text{ nm}}$ ratios were used to probe the metal ions and flavonoids, which had been studied by the CDs formed at 10 sccm (CD-10) [3]. The changes in the relative PL intensity (I/I_0) after separately adding the analytes to the three CDs were compiled in Fig. S4. For the metal ions, the 480 nm emission of CD-5 was selectively quenched by Hg^{2+} while the 410 nm emission of CD-30 was quenched by many cations, including Fe^{3+} , Cu^{2+} , Ag^+ , and Hg^{2+} . The selective quenching between CD-5 and Hg^{2+} was dynamic because the Stern-Volmer plot was linear ($R^2 = 0.9988$) and shown in Fig. S5. The pyridinic surface groups on the CD-5 were apparently more selective in the cation quenching than the hydroxyl ones on the CD-30. As shown in Fig. 5(a), the PL intensity of CD-5 at 480 nm decreased moderately with

an increase in the Hg^{2+} concentrations from 0.2 to 50 μM and also demonstrated a slight loss of PL signal at 410 nm. As shown in Fig. 5(b), the $I_{480\text{ nm}}/I_{410\text{ nm}}$ ratio presents a good linear relationship with the Hg^{2+} concentration by the linear regression equation of $I_{480\text{ nm}}/I_{410\text{ nm}} = -0.0566 [\text{Hg}^{2+}] + 3.284$ ($R^2 = 0.9969$; $[\text{Hg}^{2+}]$ in μM units). The RSD values observed at $[\text{Hg}^{2+}] = 15\ \mu\text{M}$ and blanks were nearly 1.3% and 1.1% ($n = 10$), respectively. Based on $S/N = 3$, the detection limit was calculated to be approximately 75 nM. In addition, the recoveries of 0.2, 1.0, and 5.0 μM of spiked Hg^{2+} in the sea water were $97 \pm 2\%$, $98 \pm 2\%$, and $96 \pm 3\%$, respectively ($n = 5$). Compared with the recently reported nanocarbon-based fluorescence, as shown in Table S3, the ratiometric fluorescence of the study provides a lower detection limit to analyze the sea waters. For flavonoid samples, both the 480 nm emission of CD-5 and CD-10 were selectively quenched by quercetin while both the 410 nm emission of CD-10 and CD-30 were further quenched by other flavonoids, such as hesperetin and naringenin, as shown in Fig. S4. CD-5 and CD-10 both showed a similar degree of quenching ($\approx 43\%$) of the 480 nm PL, and there was no obvious difference in the determination of quercetin in the ethanol extract of a sun-dried peel of *Citrus reticulata* cv. Chachiensis ($\approx 4.2\ \text{mg}\cdot\text{g}^{-1}$).

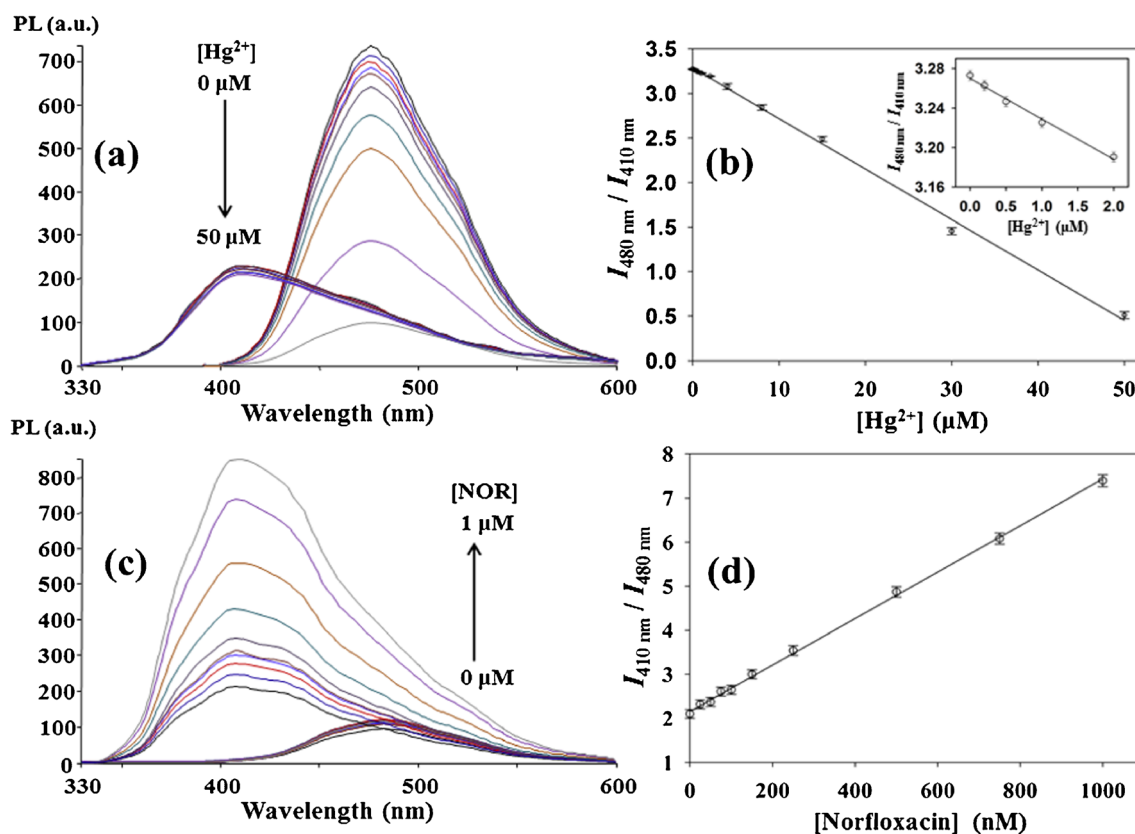


Fig. 5 Fluorescence emission spectra (a, c) and linear relationship plots (b, d) of CD-5 (a, b) and CD-30 (c, d) in the presence of different concentrations of Hg^{2+} (0, 0.2, 0.5, 1.0, 2.0, 4.0, 8.0, 15, 30, and 50 μM) (a, b) and norfloxacin (0, 25, 50, 75, 100, 150, 250, 500, 750,

1000 nM) (c, d) in 50 mM phosphate buffers (pH 7.0). The emission spectra centered approximately 410 nm and 480 nm were excited by 330 nm and 390 nm, respectively. Inset in (b) is an amplification of the linear relationship plot (b)

For CD-30, the 410 nm emission was enhanced by the addition of norfloxacin (NOR), while the 480 nm emission was evidently not affected, as shown in Fig. 5(c). The enhancement of the 410 nm emission was due to the hydrogen bond and charge transfer between NOR and the CDs emitting [27, 28]. The linear relationship between the PL intensity ratio, $I_{410 \text{ nm}}/I_{480 \text{ nm}}$, and the NOR concentration (25 nM ~ 1.0 μM) is shown as $I_{410 \text{ nm}}/I_{480 \text{ nm}} = 0.0053 [\text{NOR}] + 2.1701$ ($R^2 = 0.9992$; [NOR] in nM unit) in Fig. 5(d). The RSD values observed at 0.5 μM [NOR] and those in the blanks were nearly 2.3% and 1.2% ($n = 10$), respectively. The detection limit was calculated to be approximately 7.3 nM based on $S/N = 3$ and was comparable to other nanomaterial-based fluorescence, as shown in Table S4. Fig. S6 shows the effect of possible interferants on the relative PL intensity (I/I_0) of CDs for the determination of NOR in milk and shows the superiority of CD-30 in its sensitivity to NOR over CD-5 and CD-10. The average recoveries of NOR spiking 0.05, 0.2, and 0.5 μM NOR with CD-30 in milk were 95%, 99%, and 97% ($n = 5$). The deviation would be caused by the background UV absorption from the complex matrices of bio-samples. Furthermore, a minor limitation on the study was concerned: the excitation at two

different wavelengths can not correct the interferences from instrument fluctuation.

Conclusion

The CCP discharge of the [EMIM]N(CN)₂ solution of CA would produce a CD with excitation-independent dual-emissions at 410 nm and 480 nm. The produced CDs did not need conjugating with other fluorophores, but two excitation wavelengths were needed for measurement of the emission ratio ($I_{480 \text{ nm}}/I_{410 \text{ nm}}$). The ratio decreased with the increase in the flow rate of the O₂ plasma gas supply from 5.0 sccm to 30 sccm and with the increase in the duration of post-treatment of the CDs by UV-light and NaBH₄ reducing agent. Control of the flow rate of O₂ plasma gas at 5.0 sccm can simply tune the ratiometric fluorescence of the CDs to detect Hg^{2+} in sea water while control at 30 sccm can detect norfloxacin in milk.

Acknowledgments Support for this work by the Ministry of Science and Technology of Taiwan under Grant No. MOST-106-2113-M-039-006 and the China Medical University under Grant No. CMU106-S-17 is gratefully acknowledged.

Compliance with ethical standards The author(s) declare that they have no competing interests.

References

1. De B, Karak N (2017) Recent progress in carbon dot–metal based nanohybrids for photochemical and electrochemical applications. *J Mater Chem A* 5:1826–1859
2. Peng Z, Han X, Li S, Al-Youbi AO, Bashammakh AS, El-Shahawi MS, Leblanc RM (2017) Carbon dots: biomacromolecule interaction, bioimaging and nanomedicine. *Coord Chem Rev* 343:256–277
3. Ke C-B, Lu T-L, Chen J-L (2018) Capacitively coupled plasma discharge of ionic liquid solutions to synthesize carbon dots as fluorescent sensors. *Nanomaterials* 8:372–383
4. Zhu A, Qu Q, Shao X, Kong B, Tian Y (2012) Carbon-dot-based dual-emission nanohybrid produces a ratiometric fluorescent sensor for in vivo imaging of cellular copper ions. *Angew Chem Int Ed* 51: 7185–7189
5. Liu X, Zhang N, Bing T, Shangguan D (2014) Carbon dots based dual-emission silica nanoparticles as a ratiometric nanosensor for Cu^{2+} . *Anal Chem* 86:2289–2296
6. Lu L, Feng C, Xu J, Wang F, Yu H, Xu Z, Zhang W (2017) Hydrophobic-carbon-dot-based dual-emission micelle for ratiometric fluorescence biosensing and imaging of Cu^{2+} in liver cells. *Biosens Bioelectron* 92:101–108
7. Wang C, Lin H, Xu Z, Huang Y, Humphrey MG, Zhang C (2016) Tunable carbon-dot-based dual-emission fluorescent nanohybrids for ratiometric optical thermometry in living cells. *ACS Appl Mater Interfaces* 8:6621–6628
8. Dong Y, Cai J, Fang Q, You X, Chi Y (2016) Dual-emission of lanthanide metal–organic frameworks encapsulating carbon-based dots for ratiometric detection of water in organic solvents. *Anal Chem* 88:1748–1752
9. Wu J-X, Yan B (2017) A dual-emission probe to detect moisture and water in organic solvents based on green- Tb^{3+} post-coordinated metal–organic frameworks with red carbon dots. *Dalton Trans* 46: 7098–7105
10. Shangguan J, He D, He X, Wang K, Xu F, Liu J, Tang J, Yang X, Huang J (2016) Label-free carbon-dots-based ratiometric fluorescence pH nanoprobes for intracellular pH sensing. *Anal Chem* 88: 7837–7843
11. Zhao J, Huang M, Zhang L, Zou M, Chen D, Huang Y, Zhao S (2017) Unique approach to develop carbon dot-based nanohybrid near-infrared ratiometric fluorescent sensor for the detection of mercury ions. *Anal Chem* 89:8044–8049
12. He Y, He J, Wang L, Yu Z, Zhang H, Liu Y, Lei B (2017) Synthesis of double carbon dots co-doped mesoporous Al_2O_3 for ratiometric fluorescent determination of oxygen. *Sensors Actuators B Chem* 251:918–926
13. Yan F, Bai Z, Liu F, Zu F, Zhang R, Xu J, Chen L (2018) Ratiometric fluorescence probes based on carbon dots. *Curr Org Chem* 22:57–66
14. Barati A, Shamsipur M, Abdollahi H (2016) Carbon dots with strong excitation-dependent fluorescence changes towards pH. Application as nanosensors for a broad range of pH. *Anal Chim Acta* 931:25–33
15. Chandra A, Singh N (2017) Biocompatible fluorescent carbon dots for ratiometric intracellular pH sensing. *ChemistrySelect* 2:5723–5728
16. Wang R, Wang X, Sun Y (2017) Aminophenol-based carbon dots with dual wavelength fluorescence emission for determination of heparin. *Microchim Acta* 184:187–193
17. Zhu S, Song Y, Zhao X, Shao J, Zhang J, Yang B (2015) The photoluminescence mechanism in carbon dots (graphene quantum dots, carbon nanodots, and polymer dots): current state and future perspective. *Nano Res* 8:355–381
18. Wang W, Wang B, Embrechts H, Damm C, Cadranel A, Strauss V, Distaso M, Hinterberger V, Guldi DM, Peukert W (2017) Shedding light on the effective fluorophore structure of high fluorescence quantum yield carbon nanodots. *RSC Adv* 7:24771–24780
19. Song Y, Zhu S, Zhang S, Fu Y, Wang L, Zhao X, Yang B (2015) Investigation from chemical structure to photoluminescent mechanism: a type of carbon dots from the pyrolysis of citric acid and an amine. *J Mater Chem C* 3:5976–5984
20. Nie H, Li M, Li Q, Liang S, Tan Y, Sheng L, Shi W, Zhang SX-A (2014) Carbon dots with continuously tunable full-color emission and their application in ratiometric pH sensing. *Chem Mater* 26: 3104–3112
21. Ding H, Ji Y, Wei J-S, Gao Q-Y, Zhou Z-X, Xiong H-M (2017) Facile synthesis of red-emitting carbon dots from pulp-free lemon juice for bioimaging. *J Mater Chem B* 5:5272–5277
22. Song Y, Zhu S, Xiang S, Zhao X, Zhang J, Zhang H, Fu Y, Yang B (2014) Investigation into the fluorescence quenching behaviors and applications of carbon dots. *Nanoscale* 6:4676–4682
23. Xiong Y, Schneider J, Reckmeier CJ, Huang H, Kasák P, Rogach AL (2017) Carbonization conditions influence the emission characteristics and the stability against photobleaching of nitrogen doped carbon dots. *Nanoscale* 9:11730–11738
24. Zheng H, Wang Q, Long Y, Zhang H, Huang X, Zhu R (2011) Enhancing the luminescence of carbon dots with a reduction pathway. *Chem Commun* 47:10650–10652
25. Zhu S, Zhang J, Tang S, Qiao C, Wang L, Wang H, Liu X, Li B, Li Y, Yu W, Wang X, Sun H, Yang B (2012) Surface chemistry routes to modulate the photoluminescence of graphene quantum dots: from fluorescence mechanism to up-conversion bioimaging applications. *Adv Funct Mater* 22:4732–4740
26. Zhu S, Shao J, Song Y, Zhao X, Du J, Wang L, Wang H, Zhang K, Zhang J, Yang B (2015) Investigating the surface state of graphene quantum dots. *Nanoscale* 7:7927–7933
27. Yang M, Li H, Liu J, Kong W, Zhao S, Li C, Huang H, Liu Y, Kang Z (2014) Convenient and sensitive detection of norfloxacin with fluorescent carbon dots. *J Mater Chem B* 2:7964–7970
28. Hua J, Jiao Y, Wang M, Yang Y (2018) Determination of norfloxacin or ciprofloxacin by carbon dots fluorescence enhancement using magnetic nanoparticles as adsorbent. *Microchim Acta* 185:137–145

Publisher's note Springer Nature remains neutral with regard to jurisdictional claims in published maps and institutional affiliations.